Spectral analysis of the weighted Laplacian in slip and no-slip flows

M. Giona,* A. Adrover, and S. Cerbelli
Dipartimento di Ingegneria Chimica, Sapienza Università di Roma, via Eudossiana 18, 00184 Roma, Italy
(Received 8 May 2009; revised manuscript received 16 September 2009; published 3 December 2009)

Slip boundary conditions for the velocity field impact on the spectral properties of the advection-diffusion operator describing transport of passive particles in laminar parallel flows. By considering the Hermitian operator (referred to as the weighted Laplacian), describing the interplay between axial convection and cross-sectional diffusion of a scalar field, we show that the spectral watershed between slip and no-slip boundary conditions is a qualitatively different scaling behavior of the mean of the normalized eigenfunctions of the weighted Laplacian. The occurrence of slip conditions also influences the scaling of the density of states as regards both the leading and the subleading term in the Weyl's expansion.

DOI: 10.1103/PhysRevE.80.066302 PACS number(s): 83.50.Ha, 47.15.−x, 83.50.Rp, 05.60.−k

I. INTRODUCTION

The possible occurrence of slip velocity at static walls enclosing a laminar liquid flow is one of the main current problems in microfluidics, which admits profound implications on the validity of the continuum formulation, and specifically on the reliability of the Navier-Stokes equations at micrometric and submicrometric scales. This problem is becoming increasingly relevant, as miniaturized flow devices containing channels or capillaries of submicron characteristic diameter are becoming more and more widespread. Specifically, the occurrence of slip boundary conditions in microchannels for a liquid (aqueous) phase is the subject of ongoing scientific debate [1], and experimental results on micrometer channels performed by using microparticle image velocimetry or total internal reflection velocimetry [2] suggest, to date, contradictory conclusions (see, e.g., the review [3] and references therein).

Recently, Giona *et al.* [4] showed how the possible occurrence of slip on simple channel flows could in principle be detected from the analysis of transport properties of scalar fields advected by the flow in the presence of diffusion. The analysis developed in [4] is grounded on the behavior of the dominant Frobenius eigenvalue associated with the non-Hermitian advection-diffusion operator in channel flows. Albeit the approach proposed in [4] is very difficult to implement experimentally, its conceptual interest resides in the possibility of investigating flow properties (and specifically the onset of slip flows in microchannels) via indirect measurements of scalar concentration fields advected by the flow.

More recently, an experimentally feasible approach for detecting slip velocity in laminar flows, grounded on the application of wide-bore chromatography [5], has been proposed [6].

The results obtained in [4,6] indicate clearly that the local velocity profile near the solid walls of a microchannel impacts on the properties of linear transport operators associated with the interplay between advection and diffusion of a scalar concentration field evolving along the channel.

The aim of this article is to analyze the influence of the near-wall flow on the simplest advection-diffusion operator describing scalar field evolution in laminar channel flows. The operator considered throughout this article, namely, the Hermitian cross-sectional Laplacian operator weighted with respect to the axial velocity field (for details see Sec. II), arises naturally in the context of the moment analysis [7] of a typical hydrodynamic chromatography experiment [8].

More specifically, we seek for a characterization of the fine structure of the near-wall velocity profile in terms of the spectral properties of a Hermitian operator (referred to as the *weighted Laplacian*), which, in the present context, describes the interplay between axial convection and cross-sectional diffusion of a passive scalar embedded in a laminar carrier flow. We show that even though no relevant information can be obtained from the scaling of the eigenvalue spectrum, there are specific features associated with the structure of the eigenfunctions that are sensitive to the slip/no-slip behavior of the axial velocity. Therefore, a qualitative spectral criterion can be established for discriminating between slip and no-slip channel flows, based on the properties of the eigenfunctions. Moreover, the analysis of the density of states (DOS) of the weighted Laplacian reveals quantitative differences in the Weyl's expansion [9] in the presence of slip flows with respect to the no-slip case.

The latter problem (scaling of the density of states) bears some analogies with the seminal work by Marc Kac [10] on the detection of the shape of the boundary of a closed two-dimensional (2D) domain from the structure of the eigenfrequencies and eigenfunctions associated with the propagation of amplitude waves within the domain, and with the subsequent Literature related to the identification of fractal boundaries from the spectral properties of the Laplacian operator [11].

The article is organized as follows. Starting from a typical chromatographic experiment, Sec. II formulates the proper mathematical setting via moment analysis, and introduces the Hermitian operator associated with the interplay between transverse (cross-sectional) diffusion and axial advection in channel flows. Section III analyzes the eigenvalue/eigenfunction structure of this operator and provides a quantitative criterion for detecting the occurrence of slip boundary velocity from the properties of the eigenfunctions of the weighted Laplacian. The spectral analysis of the weighted

*Author to whom correspondence should be addressed; max@giona.ing.uniroma1.it

Laplacian operator is intrinsically theoretical, since the eigenfunction of the advection-diffusion problem are not directly (experimentally) observable. Section IV discusses the scaling of the density of states of the weighted Laplacian operator in the case of slip and no-slip flows.

II. STATEMENT OF THE PROBLEM

This section introduces the physical setting of the problem, motivated by the analysis of chromatographic experiments, and the *weighted Laplacian operator* associated with moment analysis that is considered throughout the article.

A. Solute transport in a finite-length channel

The simplest way of approaching the analysis of laminar channel flows through a transport-based experiment is to perform a chromatographic experiment [7].

Consider, for the sake of simplicity, a two-dimensional channel of length L and cross-sectional width W with $L \gg W$. Let x be the axial coordinate and y the cross-sectional coordinate $(0 \le x \le L, 0 \le y \le W)$, and $\mathbf{v}=(v(y),0)$ the axial laminar velocity profile (Poiseuille flow).

At time $t=0$, a dye (solute) is injected at the inlet section of the channel (i.e., at $x=0$) in an impulsive way [let $c(t,x,y)$ be its concentration], and at the outlet section (i.e., at $x=L$) its average concentration profile is recorded as a function of time t.

The evolution of the scalar field $c(t,x,y)$ within the channel can be modeled via the advection-diffusion equation

$$\frac{\partial c}{\partial t} = -v(y)\frac{\partial c}{\partial x} + \mathcal{D}\left(\frac{\partial^2 c}{\partial x^2} + \frac{\partial^2 c}{\partial y^2}\right), \tag{1}$$

where $\mathcal{D}$ is the diffusivity of the solute. By making the formulation nondimensional, and letting $\phi = c/C_{\mathrm{ref}}$, $v(y) = V_{\mathrm{ref}}u(y)$, $x \to x/L$, $y \to y/W$, and $t \to tV_{\mathrm{ref}}/L$ (henceforth we will use x, y, and t as the above defined dimensionless variables), where C_{ref} is a reference concentration, V_{ref} a reference velocity [so that $u(y)$ admits unit average velocity $\int_0^1 u(y)dy = 1$], Eq. (1) becomes

$$\frac{\partial \phi}{\partial t} = -u(y)\frac{\partial \phi}{\partial x} + \frac{1}{\mathrm{Pe}}\left(\frac{\partial^2 \phi}{\partial x^2} + \alpha^2\frac{\partial^2 \phi}{\partial y^2}\right), \tag{2}$$

where $0 < x,y < 1$, $\mathrm{Pe} = V_{\mathrm{ref}}L/\mathcal{D}$ is the Péclet number referred to the channel length, and $\alpha = L/W \gg 1$ the channel aspect ratio. Equation (2) is equipped with vanishing initial condition $\phi(t,x,y)|_{t=0}=0$, and impulsive inlet condition $\phi(t,x,y)|_{x=0}=\delta(t)$. Solid walls are impermeable to mass transport, and therefore the homogeneous Neumann conditions apply, i.e., $\partial\phi(t,x,y)/\partial y|_{y=0,1}=0$. As regards the outlet boundary condition, different choices are possible. A typical approach is to consider the infinite-length approximation, i.e., the column is regarded as infinitely extended, $x \in (0,\infty)$, (so that solely the regularity condition at infinity applies), but the outlet concentration profile is evaluated at $x=1$, i.e., at the outlet section of the capillary. Alternatively, one may use the Danckwerts' outlet boundary condition that dictates $\partial\phi(t,x,y)/\partial x|_{x=1}=0$, i.e., the outlet solute flux is purely convective. Since in this article attention is focused on relatively high Péclet numbers (i.e., $\mathrm{Pe}/\alpha^2 > 1$, with $\alpha \gg 1$), the outlet condition is practically irrelevant since the contribution of axial dispersion is negligible in this parameter region. With the present normalization, the interplay between axial advection and diffusion, and the role of the channel geometry is characterized by two dimensionless groups: the Péclet number Pe defined above with respect to the channel length L, and the *effective Péclet number* $\mathrm{Pe}_{\mathrm{eff}} = \mathrm{Pe}/\alpha^2$. The latter quantity expresses the ratio of the characteristic diffusion time along the cross section of the channel $t_{\mathrm{diff,cross}} = W^2/\mathcal{D}$, and the axial advection time $t_{\mathrm{adv,axial}} = L/V_{\mathrm{ref}}$, since

$$\mathrm{Pe}_{\mathrm{eff}} = \frac{\mathrm{Pe}}{\alpha^2} = \frac{V_{\mathrm{ref}}W^2}{\mathcal{D}L} = \frac{t_{\mathrm{diff,cross}}}{t_{\mathrm{adv,axial}}}. \tag{3}$$

The target quantity in chromatography is therefore the function

$$\phi_o(t) = \int_0^1 \phi(t,1,y)dy, \tag{4}$$

which corresponds to the average outlet concentration. At fixed aspect ratio α of the column and increasing Pe values, the dispersion properties of the solute are first characterized by the *Taylor-Aris dispersion* [12,8], and subsequently (at higher Pe) by a *convection-dominated* dispersion regime [6,13]. The transition between these two different dispersion regimes becomes evident from the visual inspection of the graph of the outlet chromatograms $\phi_o(t)$ depicted in Fig. 1. In the Taylor-Aris regime (curve a) the outlet chromatogram possesses an almost Gaussian profile centered close to $t=1$. As Pe increases, the transition toward the convection-dominated regime occurs, characterized by a highly asymmetric shape of $\phi_o(t)$ (curve b), whose modal abscissa t_{mod} (i.e., the time instant of the peak) becomes progressively located at $t_{\mathrm{min}} = 1/u_{\mathrm{max}}$, where $u_{\mathrm{max}} = \max_y u(y)$, that for 2D channel flow $[u(y)=6y(1-y)]$ corresponds to $t_{\mathrm{min}}=2/3$. Physically, this corresponds to the fact that downstream diffusion becomes less and less important with respect to axial convection. For high values of Pe, the outlet chromatogram

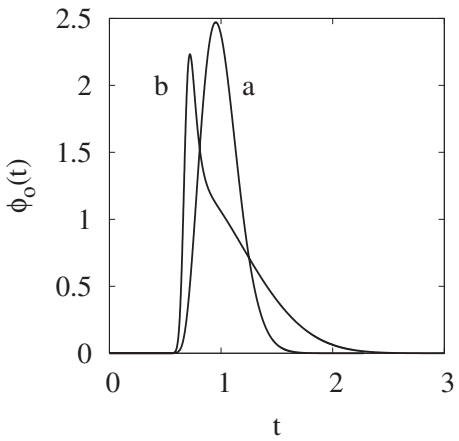

FIG. 1. Outlet chromatogram $\phi_o(t)$ vs t for $\alpha=20$. Transition from Taylor-Aris to convection-dominated regime. Line (a) $\mathrm{Pe}=1000$ ($\mathrm{Pe}_{\mathrm{eff}}=2.5$), line (b) $\mathrm{Pe}=5000$ ($\mathrm{Pe}_{\mathrm{eff}}=12.5$).

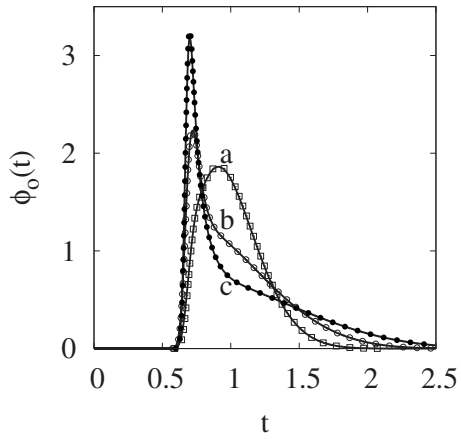

FIG. 2. Comparison between the solution of Eq. (2) (solid lines) and the solution of Eq. (5) (symbols) obtained neglecting axial diffusion at $\alpha=20$, at different Pe values. Line (a) and (□) Pe=2000 ($Pe_{eff}=5$), line (b) and (○) Pe=5000 ($Pe_{eff}=12.5$), line (c) and (●) Pe=10000 ($Pe_{eff}=25$).

$\phi_o(t)$ approaches the purely kinematic residence-time probability density functions (i.e., the time necessary for a solute particle initially located at the channel inlet to reach the outlet section while driven exclusively by advection). This is a first heuristic indication that, starting from a chromatographic experiment performed at a sufficiently large Pe value, it is possible to recover information on the channel velocity $u(y)$. The analysis of the convection-dominated dispersion regime is out of the scope of the present article and it is addressed in detail in [6]. The experimental use of chromatographic columns for analytical purposes operating in the convection-dominated regime has been recently introduced in chemical practice and is referred to as *wide-bore* chromatography [5].

For high Péclet values, such as $Pe_{eff} \geq 5$ [14], the effect of axial dispersion on the shape of the outlet chromatogram becomes negligible, and the term $\partial^2\phi/\partial x^2$ in Eq. (2) can be dropped out. Numerical evidence for the validity of this approximation is depicted in Fig. 2. Therefore, Eq. (2) simplifies to

$$\frac{\partial \phi}{\partial t} = -u(y)\frac{\partial \phi}{\partial x} + \varepsilon \frac{\partial^2 \phi}{\partial y^2}. \tag{5}$$

In Eq. (5) we have introduced the parameter $\varepsilon=\alpha^2/\mathrm{Pe}=1/\mathrm{Pe}_{\mathrm{eff}}$.

In the case of a circular capillary of radius R and length L, letting $\rho=r/R$, and z the dimensionless normalized axial coordinate, $z \in (0,1)$, the counterpart of Eq. (5) for a radially symmetric inlet reads

$$\frac{\partial \phi}{\partial t} = -u(\rho)\frac{\partial \phi}{\partial z} + \frac{\varepsilon}{\rho}\frac{\partial}{\partial \rho}\left(\rho \frac{\partial \phi}{\partial \rho}\right), \tag{6}$$

where $\alpha=L/R$, and ε and Pe are defined as in the case of the 2D channel.

B. Moment analysis and axially weighted Laplacian

The relevant information on transport properties of the solute associated with the outlet average concentration $\phi_o(t)$ is recovered by the moment hierarchy $m_{\mathrm{out}}^{(n)}$ defined as

$$m_{\mathrm{out}}^{(n)} = \int_0^\infty t^n \phi_o(t)dt = \int_0^\infty t^n dt \int_0^1 \phi(t,1,y)dy, \quad n=0,1,\ldots \tag{7}$$

and by considering the first elements $n=1,2$ of this hierarchy [15].

By introducing the local moments $m^{(n)}(x,y)$ defined as

$$m^{(n)}(x,y) = \int_0^\infty t^n \phi(t,x,y)dt, \tag{8}$$

it follows that $m_{\mathrm{out}}^{(n)}=\int_0^1 m^{(n)}(1,y)dy$. For $\mathrm{Pe}/\alpha^2 \geq 5$, i.e., when axial diffusion becomes negligible, the local moments $m^{(n)}(x,y)$ satisfy the system of parabolic equations

$$u(y)\frac{\partial m^{(n)}(x,y)}{\partial x} = \varepsilon \frac{\partial^2 m^{(n)}(x,y)}{\partial y^2} + n m^{(n-1)}(x,y), \tag{9}$$

where, in the case of an impulsive loading, $m^{(0)}(x,y)=1$ and $m^{(n)}(0,y)=0$ for $n=1,2,\ldots$. For a circular capillary, the moment hierarchy $m^{(n)}(z,\rho)$ satisfies the equation

$$u(\rho)\frac{\partial m^{(n)}(z,\rho)}{\partial z} = \frac{\varepsilon}{\rho}\frac{\partial}{\partial \rho}\left(\rho \frac{\partial m^{(n)}(z,\rho)}{\partial \rho}\right) + n m^{(n-1)}(z,\rho), \tag{10}$$

and the outlet moments $m_{\mathrm{out}}^{(n)}$ are related to $m^{(n)}(z,\rho)$ by the equation

$$m_{\mathrm{out}}^{(n)} = 2\int_0^1 \rho m^{(n)}(z,\rho)d\rho. \tag{11}$$

Consider again Eq. (9), and let $\zeta=\varepsilon x$. From Eq. (9) one obtains

$$u(y)\frac{\partial m^{(n)}(\zeta,y)}{\partial \zeta} = \frac{\partial^2 m^{(n)}(\zeta,y)}{\partial y^2} + \frac{n}{\varepsilon} m^{(n-1)}(\zeta,y), \tag{12}$$

and the outlet moments are thus expressed by the equations

$$m_{\mathrm{out}}^{(n)} = \int_0^1 m^{(n)}(\varepsilon,y)dy. \tag{13}$$

Equation (12) indicates that all the information about the moment hierarchy is embedded in the spectral properties of the weighted Laplacian operator

$$\mathcal{L}_u[\psi] = \frac{1}{u(y)}\frac{d^2\psi}{dy^2}, \tag{14}$$

i.e., within the eigenvalue/eigenfunction spectrum associated with the generalized eigenvalue problem

$$-\lambda u(y)\psi(y) = \frac{d^2\psi(y)}{dy^2} \quad \psi'(0)=\psi'(1)=0, \tag{15}$$

which is the main object of investigation of the present article.

C. Channel flows and slip boundary conditions

Before addressing the spectral properties of $\mathcal{L}_u$ and how they depend on $u(y)$ (or on $u(\rho)$, for circular channels), let us briefly recall how the occurrence of slip velocity for a laminar flow in a two-dimensional channel can be described by means of the Navier boundary condition

$$\gamma \frac{du(y)}{dn_e} = -u(y)|_{y=0,1}, \tag{16}$$

where n_e is the outward normal direction to the channel walls (located at $y=0$ and $y=1$), and $\gamma=\ell_s/W$ is the dimensionless slip length (ℓ_s is the slip length, *sensu stricto*, that in liquid microflows may attain values between ten nanometers and few microns, depending on the liquid phase, the structure and the material forming the channel walls, and the way the measurement is performed, as discussed in [3]). In a two-dimensional channel flow, the normalized axial velocity profile is therefore expressed by

$$u(y) = \frac{6}{1+6\gamma}(y - y^2 + \gamma). \tag{17}$$

The prefactor $6/(1+6\gamma)$ entering Eq. (17) ensures unit average velocity. For $\gamma=0$ one recovers the no-slip Poiseuille profile.

In a similar way, the normalized axial velocity profile in a circular channel with slip reads as

$$u(\rho) = \frac{2}{1+2\gamma}(1 + \gamma - \rho^2), \tag{18}$$

where $\gamma=\ell_s/R$.

Next, we show how from the spectral structure of $\mathcal{L}_u$ it is possible to discriminate between the two cases $\gamma=0$ and $\gamma>0$.

III. SPECTRAL STRUCTURE OF THE WEIGHTED LAPLACIAN

A. General properties of the weighted Laplacian

Consider the eigenvalues and the eigenfunctions of the weighted Laplacian $\mathcal{L}_u$ defined by Eqs. (14) and (15). Let $\langle f,g\rangle=\int_0^1 f(y)\bar{g}(y)dy$, $\langle f,g\rangle_u=\int_0^1 u(y)f(y)\bar{g}(y)dy$ (where $\bar{g}$ is the complex conjugate of g). $\mathcal{L}_u$ is a Hermitian operator and therefore its eigenvalues are all real and nonpositive since

$$\lambda_h = \frac{\langle \psi_h', \psi_h' \rangle}{\langle \psi_h, \psi_h \rangle_u} \geq 0, \quad h = 0,1,\ldots, \tag{19}$$

where ψ_h is the real-valued eigenfunction associated with λ_h and $\psi_h'(y)=d\psi_h(y)/dy$ (observe that the eigenvalue of $\mathcal{L}_u$ is $-\lambda_h$), verifying Neumann boundary conditions at the channel walls.

By ordering the spectrum $\{\lambda_h\}_{h=0}^{\infty}$ in an increasing way, it follows that $\lambda_0=0$ which corresponds the uniform eigenfunction $\psi_0(y)=1$, while $\lambda_h>0$ for $h=1,2,\ldots$.

The eigenfunctions are orthogonal with respect to the weighted inner product,

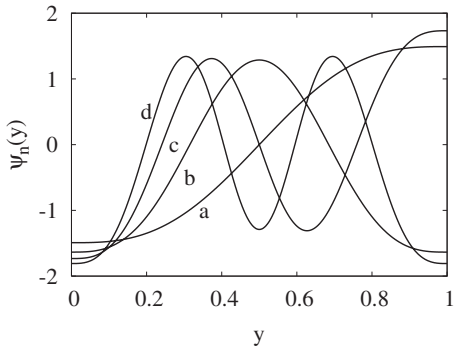

FIG. 3. The first four nonuniform eigenfunctions $\psi_n(y)$, $n=1,2,3,4$ (lines from (a) to (d)) for a 2D no-slip channel flow.

$$\langle \psi_h, \psi_k \rangle_u = \int_0^1 u(y)\psi_h(y)\psi_k(y)dy = 0, \quad h \neq k \tag{20}$$

and can be assumed to be normalized, i.e., $\|\psi_h\|_u^2=\langle \psi_h, \psi_h\rangle_u=1$. Moreover, they form a basis for the space $L_u^2([0,1])$ of the square summable functions with respect to the weight $u(y)$,

$$L_u^2([0,1]) = \{f(y) | \langle f,f\rangle_u < \infty\}. \tag{21}$$

This implies that any $f \in L_u^2([0,1])$ can be expanded in a convergent series of eigenfunctions

$$f(y) = \sum_{n=0}^{\infty} f_n \psi_n(y), \quad f_n = \langle f, \psi_n \rangle_u. \tag{22}$$

Figure 3 shows the first four nonconstant eigenfunctions [16] $\psi_n(y)$ for the 2D channel flow Eq. (17) with $\gamma=0$ (no slip).

The case of circular channel flow is almost identical. The eigenfunction problem in cylindrical coordinates reads

$$-\lambda_h u(\rho)\psi_h(y) = \frac{1}{\rho}\frac{d}{d\rho}\left(\rho \frac{d\psi_h}{d\rho}\right), \tag{23}$$

and

$$\lambda_h = \frac{\langle \psi_h', \psi_h' \rangle_\rho}{\langle \psi_h, \psi_h \rangle_{\rho u}} \geq 0, \quad h = 0,1,\ldots, \tag{24}$$

where $\langle f,g\rangle_\rho=\int_0^1 \rho f(\rho)\bar{g}(\rho)d\rho$, $\langle f,g\rangle_{\rho u}=\int_0^1 \rho u(\rho)f(\rho)\bar{g}(\rho)d\rho$. Consequently, instead of Eq. (22), the generalized Fourier expansion for any function $f \in L_{\rho u}^2([0,1])$ reads

$$f(\rho) = \sum_{n=0}^{\infty} f_n \psi_n(\rho), \quad f_n = \langle f, \psi_n \rangle_{\rho u}. \tag{25}$$

Let us consider the eigenvalue spectrum. Figure 4 depicts the eigenvalue spectrum for 2D (panel A) and for circular channel flow (panel B) for different values of γ. As can be observed, there is neither qualitative nor significant quantitative difference between the eigenvalue spectra associated with axial velocity profiles $u(y)$ [and $u(\rho)$ for circular capillaries] for zero and small values of γ. For large n, the classical scaling

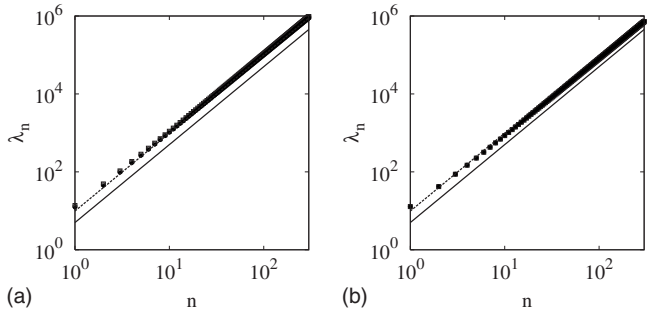

FIG. 4. Eigenvalue spectrum $\{\lambda_n\}$ vs n associated with the weighted Laplacian. (a) 2D channel flow: (□) $\gamma=0$ (no-slip flow), (○) $\gamma=0.03$, (●) $\gamma=0.1$. (b) Flow in a circular capillary: (□) $\gamma=0$ (no-slip Poiseuille flow), (○) $\gamma=0.03$, (●) $\gamma=0.1$. The solid lines represent the scaling $\lambda_n \sim n^2$. The dashed lines depict $\lambda_n = \pi^2 n^2$.

$$\lambda_n \sim n^2 \tag{26}$$

is observed independently of γ. This means that it is not possible to discriminate between slip and no-slip flow conditions at the solid walls on the basis of the eigenvalue spectrum. Therefore, any attempt of spectral discrimination should be grounded on the properties of the eigenfunctions, and this is discussed in the next paragraph. Alternatively, quantitative differences between slip and no-slip flows can be observed in the global spectral properties, expressed, e.g., by the density of states, as discussed in Sec. IV.

B. First-order moments

A feasible way of discriminating between slip and no-slip conditions in channel flows by a chromatographic experiment can be based on the analysis of first-order moments $m_{\text{out}}^{(1)}$ and $m_{\text{out}}^{(2)}$ and of their dependence on $\text{Pe}_{\text{eff}}=1/\varepsilon=\text{Pe}/\alpha^2$ [6]. For the scope of the present analysis, it is sufficient to consider exclusively the first-order moment $m_{\text{out}}^{(1)}$. Figure 5 shows the behavior of $m_{\text{out}}^{(1)}$ as a function of the effective Péclet number Pe_{eff}. In the case of no-slip conditions, $m_{\text{out}}^{(1)}(\text{Pe}_{\text{eff}})$ diverges with Pe_{eff}, while for any $\gamma>0$ (slip flows) $m^{(1)}(\text{Pe}_{\text{eff}})$ saturates toward a constant value.

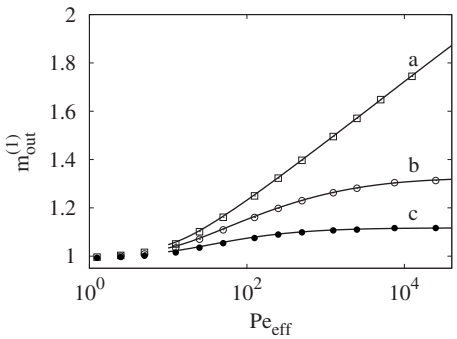

FIG. 5. First-order moment $m_{\text{out}}^{(1)}$ vs the effective Péclet number Pe_{eff} for the 2D channel flow. Lines represent the results of Eqs. (7)–(9) for $n=1$, symbols those obtained form numerical simulations of the advection-diffusion Eq. (2). Line (a) and (□) $\gamma=0$ (no-slip), line (b) and (○) $\gamma=0.03$, line (c) and (●) $\gamma=0.1$.

These results can be easily interpreted, since for $\text{Pe}_{\text{eff}} \to \infty$ (i.e., for $\varepsilon \to 0$), the outlet chromatogram $\phi_o(t)$ converges toward the kinematic residence-time distribution $p_T(t)$ that, for uniform inlet injection (i.e., whenever the solute in injected uniformly along the inlet cross section), is $p_T(t)=0$ for $t<t_{\min}$, and

$$p_T(t) = \frac{2}{C_\gamma t}\frac{1}{\sqrt{(1+4\gamma)t^2 - 4t/C_\gamma}}, \quad \text{for} \quad t_{\min}(\gamma) \le t \le t_{\max}(\gamma), \tag{27}$$

where $C_\gamma=6/(1+6\gamma)$, $t_{\min}(\gamma)=2(1+6\gamma)/3(1+4\gamma)$, and $t_{\max}(\gamma)=1+1/6\gamma$.

For $\gamma=0$, i.e., in the presence of no-slip velocity profile, Eq. (27) reduces to

$$p_T(t) = \frac{1}{t\sqrt{9t^2-6t}}, \quad t \ge 2/3. \tag{28}$$

Therefore, for $\varepsilon \to 0$, and γ arbitrary,

$$\begin{aligned}\lim_{\varepsilon\to 0} m_{\text{out}}^{(1)} &= \frac{2}{C_\gamma}\int_{t_{\min}}^{t_{\max}} \frac{dt}{\sqrt{(1+4\gamma)t^2 - 4t/C_\gamma}} \\ &= \frac{2}{C_\gamma\sqrt{1+4\gamma}}\log(2\sqrt{(1+4\gamma)[(1+4\gamma)t^2 - 4t/C_\gamma]} \\ &\quad + 2(1+4\gamma)t - 4/C_\gamma)\big|_{t=t_{\min}(\gamma)}^{t_{\max}(\gamma)}.\end{aligned} \tag{29}$$

For any $\gamma>0$, $m_{\text{out}}^{(1)}$ is bounded, while it diverges at $\gamma=0$ (see Fig. 5). Specifically, for small γ, Eq. (29) shows that $m_{\text{out}}^{(1)} \sim -\log(\gamma)/3$.

In order to analyze how the presence of slip conditions impacts upon the structure of the eigenfunctions of the weighted Laplacian, the analysis of the first-order moment provides a useful starting point.

C. c spectrum

Equation (12) for $m^{(1)}(\zeta,y)$ reads

$$u(y)\frac{\partial m^{(1)}(\zeta,y)}{\partial \zeta} = \frac{\partial^2 m^{(1)}(\zeta,y)}{\partial y^2} + \varepsilon^{-1}, \tag{30}$$

and the average outlet first-order moment is $m_{\text{out}}^{(1)} = \int_0^1 m^{(1)}(\varepsilon,y)dy$. By expanding $m^{(1)}(\zeta,y)$ with respect to the eigenbasis of the weighted Laplacian, $m^{(1)}(\zeta,y) = \Sigma_{h=0}^{\infty} m_h^{(1)}(\zeta)\psi_h(y)$, one obtains for $m_h^{(1)}(\zeta)$ the system of differential equations

$$\frac{dm_h^{(1)}(\zeta)}{d\zeta} = -\lambda_h m_h^{(1)} + \varepsilon^{-1} d_h, \tag{31}$$

where

$$d_h = \int_0^1 \psi_h(y)dy. \tag{32}$$

The sequence $\{c_h\}_{h=0}^{\infty}$, where $c_h=|d_h|$, will be referred to as the *c spectrum* associated with the operator $\mathcal{L}_u$. Equations (31) can be solved yielding $m_0^{(1)}(\zeta)=\varepsilon^{-1}$, since $d_0=1$, and

$$m_h^{(1)}(\zeta) = \frac{d_h}{\varepsilon\lambda_h}(1 - e^{-\lambda_h\zeta}), \quad h = 1,2,\ldots. \tag{33}$$

Therefore, the first-order moment $m_{\text{out}}^{(1)}$ can be expressed as

$$m_{\text{out}}^{(1)} = 1 + \sum_{h=1}^{\infty} \frac{c_h^2}{\varepsilon\lambda_h}(1 - e^{-\lambda_h\varepsilon}). \tag{34}$$

Since for small γ, $\lambda_h \simeq \pi^2 h^2$, independently of γ (this result stems from the fact that in the case of pure diffusion, i.e., no axial flow, the eigenvalues of the Laplacian operator equipped with the Neumann boundary condition in [0,1] are $\lambda_h = \pi^2 h^2$; for a numerical validation see the dashed lines in Fig. 4), the properties of $m_{\text{out}}^{(1)}$ are controlled by the scaling of the c spectrum. By enforcing the simplification $\lambda_h = \pi^2 h^2$, Eq. (34) reduces to

$$m_{\text{out}}^{(1)} \simeq 1 + \sum_{h=1}^{\infty} \frac{c_h^2}{\varepsilon\pi^2 h^2}(1 - e^{-\varepsilon\pi^2 h^2}). \tag{35}$$

Since,

$$\frac{(1 - e^{-\varepsilon\pi^2 h^2})}{\varepsilon\pi^2 h^2} \simeq \begin{cases} 1, & h < N^*(\varepsilon) \\ 1/(\varepsilon\pi^2 h^2), & h > N^*(\varepsilon), \end{cases} \tag{36}$$

where $N^*(\varepsilon) = (\varepsilon\pi^2)^{-1/2}$. The first-order moment $m_{\text{out}}^{(1)}$ can be approximated as

$$m_{\text{out}}^{(1)} = \simeq 1 + \sum_{h=1}^{|N^*(\varepsilon)|} c_h^2 + \sum_{h=|N^*(\varepsilon)|+1}^{\infty} \frac{c_h^2}{\varepsilon\pi^2 h^2}$$

$$= 1 + \sum_{h=1}^{|N^*(\varepsilon)|} c_h^2 + r(\varepsilon) = S^*(\varepsilon) + r(\varepsilon), \tag{37}$$

where $|N^*(\varepsilon)|$ is the closest integer to $N^*(\varepsilon)$, and $r(\varepsilon)$ is the last residual summation in the first Eq. (37). For $\varepsilon \to 0$, the residual approaches a constant value $\lim_{\varepsilon\to 0} r(\varepsilon) = r_0 \sim \mathcal{O}(10^{-1})$ [17]. Therefore, to the leading order, the scaling of the first-order moment is controlled by the function $S^*(\varepsilon)$.

Two cases should be considered. For $\gamma > 0$, $m_{\text{out}}^{(1)}$ is bounded, and from Eq. (37) the sum $\Sigma_{h=1}^{\infty} c_h^2$ should be convergent. This means that c_h^2 goes to zero faster that h^{-1}, i.e., $c_h \sim K h^{-(1/2+\beta)}$ for some $K > 0$ and $\beta > 0$.

Conversely, for $\gamma = 0$, $m_{\text{out}}^{(1)}$ diverges to infinity for $\varepsilon \to 0$, and the c spectrum should decay as $c_h \sim K h^{-(1/2-\beta)}$ for some $K > 0$ and $\beta \geq 0$. The scaling of c_h for 2D slip and no-slip flows is depicted in Fig. 6(a). In the case of the Poiseuille flow one observes that $c_{2h+1} = 0$ [and this may be due to the symmetry of the axial velocity $u(y)$ around $y = 1/2$], and solely even-order terms c_{2h} are different from zero. Numerical simulations indicate that

$$c_{2h} \sim h^{-1/2}, \tag{38}$$

for no-slip Poiseuille flow, while

$$c_{2h} \sim h^{-2}, \tag{39}$$

for a channel flow in the presence of slip velocity at the walls. Indeed, from Eqs. (37) and (38) it follows that $m_{\text{out}}^{(1)}$ possesses a logarithmic divergence with Pe_{eff} for no-slip Poiseuille flow, $m_{\text{out}}^{(1)} \sim C \log(\text{Pe}_{\text{eff}})$, where C is a constant, as observed in the numerical simulations (Fig. 5). An identical result holds for circular capillaries [see Fig. 6(b)], with the only difference that in cylindrical structures with circular cross section the c spectrum is defined as

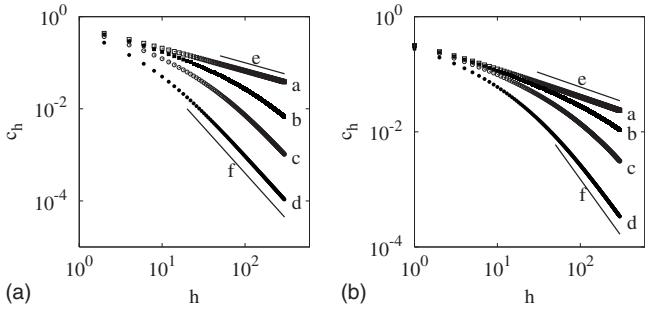

FIG. 6. Scaling of the c-spectrum c_h vs h. (a) 2D channel flow. (a) $\gamma = 0$ (no-slip), (b) $\gamma = 0.01$, (c) $\gamma = 0.03$, (d) $\gamma = 0.1$. (b) Flow in a circular capillary. (a) $\gamma = 0$ (no-slip Poiseuille flow), (b) $\gamma = 0.01$, (c) $\gamma = 0.03$, (d) $\gamma = 0.1$. Lines (e) and (f) are the scalings $c_h \sim h^{-1/2}$ and $c_h \sim h^{-2}$, respectively.

$$c_h = \left| \int_0^1 \rho\psi_h(\rho)d\rho \right|. \tag{40}$$

The validity of the above analysis is further confirmed by the following prediction. From the behavior of c_h in 2D channel flow the following approximation $c_{2h} = C_0(2h)^{-1/2}$, where $C_0 = 0.655$ can be applied [Fig. 7(a)]. From Eq. (37) it follows that the sum $\Sigma(\text{Pe}_{\text{eff}})$ defined by

$$\Sigma(\text{Pe}_{\text{eff}}) = 1 + C_0^2 \sum_{h=1}^{|N^*(\varepsilon)/2|} \frac{1}{2h} \tag{41}$$

provides an approximation for $m_{\text{out}}^{(1)}$ for high values of Pe_{eff}. Figure 7(b) depicts the comparison of $m_{\text{out}}^{(1)}$ and $\Sigma(\text{Pe}_{\text{eff}})$, revealing the good agreement between theory and simulations, as regards the scaling of the first-order moment.

The above analysis indicates that the eigenfunction structure carries information on the slip/no-slip boundary condition in channel flow, and this information is captured by the scaling of the c spectrum.

Physically, a slower decay of $\{c_h\}_{h=0}^{\infty}$ is associated with the decay of the mean value of the higher-order eigenfunctions

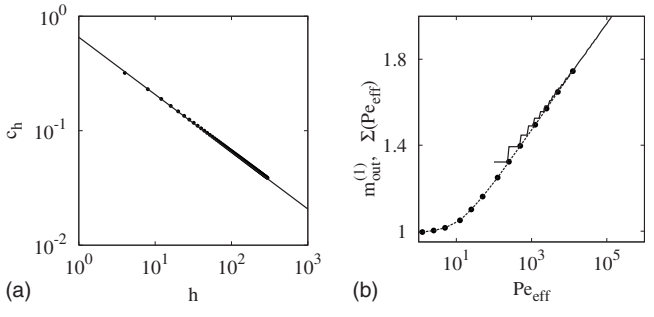

FIG. 7. (a) c_h vs h (●) and the approximation $c_h = 0.655h^{-1/2}$ (solid line). (b) Comparison of $m_{\text{out}}^{(1)}$ (●) and the partial sum $\Sigma^*(\text{Pe}_{\text{eff}})$ Eq. (41) (solid line).

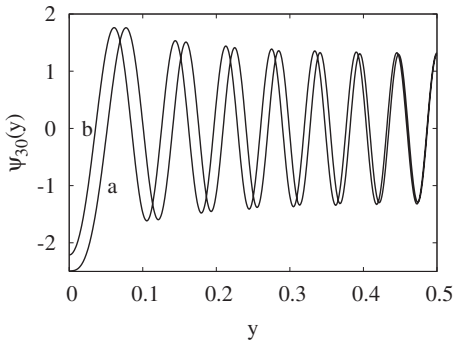

FIG. 8. Comparison of a higher-order eigenfunction $\psi_{30}(y)$ for no-slip (line a) and slip (line b) 2D channel flows (with $\gamma=0.03$).

$\psi_h(y)$ as a function of h. In the presence of no-slip Poiseuille flow, the mean value of even-order eigenfunctions $\psi_{2h}(y)$ decays to zero slower than for slip flows, and a qualitatively different scaling of c_h is observed. Figure 8 depicts two typical higher-order eigenfunctions $(2h=30)$ for no-slip and slip Poiseuille flow. Although qualitatively similar, the two eigenfunctions differ in their mean values and this influences the asymptotic scaling of the c spectra.

It is possible to give an analytical interpretation of the scaling results found above, in terms of the singularities of the reciprocal of the axial velocity field. Consider the generalized Fourier series associated with the coefficient spectrum $\{d_h\}_{h=0}^{\infty}$ (the absolute value of which is $\{c_h\}_{h=0}^{\infty}$)

$$S(y)=\sum_{n=0}^{\infty} d_n\psi_n(y). \tag{42}$$

Since

$$d_n=\int_0^1 \psi_n(y)dy=\int_0^1 u(y)\left(\frac{1}{u(y)}\right)\psi_n(y)dy, \tag{43}$$

it follows that $\{d_h\}_{h=0}^{\infty}$ is the coefficient spectrum associated with the function $1/u(y)$, i.e., with the reciprocal of the weight $u(y)$ that corresponds to the axial velocity profile. Therefore, the series Eq. (42) converges to the reciprocal of the axial velocity field in the L_u^2 metrics, i.e.,

$$\lim_{N\to\infty}\left\|\frac{1}{u(y)}-\sum_{n=0}^{N} d_n\psi_n(y)\right\|_u=0, \tag{44}$$

at any point y of continuity of $u(y)$. The comparison of $S(y)$ (truncated up to $N=300$ eigenmodes) and $1/u(y)$ is depicted in Figs. 9(a) and 9(b) for slip and no-slip channel flows, respectively. For slip flows, $1/u(y)$ is a bounded and differentiable function of its argument in (0,1). Because of the symmetry of $u(y)$ with respect to $y=1/2$, one observes the decay of the Fourier coefficients c_{2h} expressed by Eq. (39). Conversely, in no-slip Poiseuille flows $1/u(y)$ is singular at the boundaries $(y=0,1)$, and the function $1/u(y)$ is not square summable in $L_u^2([0,1])$, since $\|1/u(y)\|_u^2=\int_0^1 dy/u(y)=\infty$. As a consequence, the Parseval series $\Sigma_{h=0}^{\infty}c_h^2$ diverges, and this explains the scaling observed for no-slip flows, expressed by Eq. (38), since $1/u(y)$ does not belong to $L_u^2([0,1])$, while $1/u^{\beta}(y)$ for $\beta<1$ does.

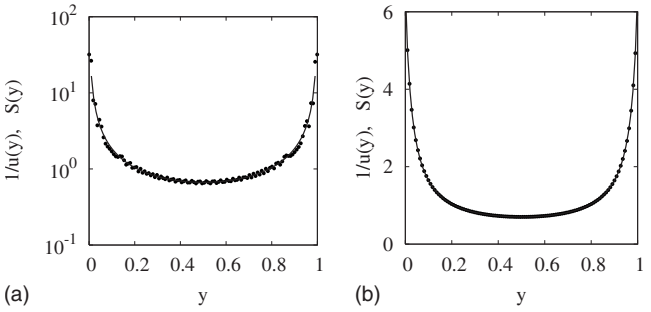

FIG. 9. $1/u(y)$ (solid lines) and $S(y)$ Eq. (42) (symbols ●) for 2D channel flows. (a) $\gamma=0$ no-slip. (b) $\gamma=0.03$.

IV. SCALING OF THE DENSITY OF STATES OF THE WEIGHTED LAPLACIAN

The classical spectral theory considers the density of states of the Laplacian operator [9,18],

$$\nabla^2\psi=-\lambda\psi, \tag{45}$$

equipped with the Dirichlet or Neumann conditions at the boundary of a closed and connected domain. Introducing $\lambda=k^2$, the density of states $N_{\mathrm{DOS}}(k,d)$ of the Laplacian operator in a d-dimensional domain [$N_{\mathrm{DOS}}(k,d)$ is a counting function, which for fixed k returns the number of eigenvalues λ such that $\lambda\le k^2$] can be expressed in the form of the asymptotic (Weyl's) expansion

$$N_{\mathrm{DOS}}(k,d)=b(d)k^d+c(d)k^{d-1}+o(k^{d-1}), \tag{46}$$

where $b(1)=L/\pi$, $b(2)=S/4\pi$, $b(3)=V/6\pi^2$, L, S, V be the d-dimensional $(d=1,2,4)$ measures of the domain [9,18]. The next to the leading-order prefactor $c(d)$ is positive for the Neumann and negative for the Dirichlet boundary conditions. In the case of the unit interval, the leading term is thus $N_0(k)=k/\pi$, and $c(1)$ is positive $[c(1)=1/2]$ for the Neumann conditions.

The spectral characterization of dispersion in straight channels involving the weighted Laplacian operator is slightly different from the classical problem reviewed above, as it is related to the generalized eigenvalue problem

$$\nabla^2\psi(\mathbf{x})=-\lambda u(\mathbf{x})\psi(\mathbf{x}),\quad \mathbf{x}\in\Sigma, \tag{47}$$

where Σ is either an interval, or a connected two-dimensional domain (representing the cross section of the channel), equipped always (i.e., both for slip and no-slip flows) with the Neumann boundary conditions (associated with the impermeability of the walls to mass flow)

$$\left.\frac{\partial\psi(\mathbf{x})}{\partial n}\right|_{\mathbf{x}\in\partial\Sigma}=0 \tag{48}$$

at the boundary $\partial\Sigma$ of Σ.

What makes the difference between slip and no-slip flows is the nature of $u(\mathbf{x})$, that is, the axial velocity field. Indeed, since creeping flow (Stokes regime) is considered, $u(\mathbf{x})$ is the solution of a Poisson equation on Σ,

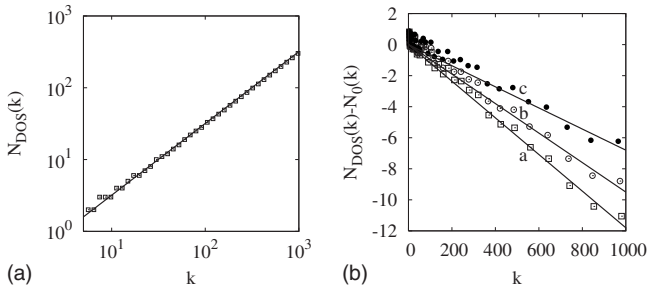

FIG. 10. (a) Density of states $N_{\mathrm{DOS}}(k)$ vs k (symbols □) for the no-slip 2D Poiseuille flow. The solid line represents the function $N_0(k)=k/\pi$. (b) $N_{\mathrm{DOS}}(k)-N_0(k)$ vs k for the no-slip and slip 2D Poiseuille flows. Symbols (□) refer to $\gamma=0$ (no-slip), (○) to $\gamma=0.01$, (●) $\gamma=0.03$. The solid lines (a) to (c), represent the functions $N_{\mathrm{DOS}}(k)-N_0(k)=-a(\gamma)k$, for $\gamma=0$, 0.01, 0.03, respectively.

$$\nabla^2 u = -A \quad , \tag{49}$$

where A is a constant (related to the pressure gradient), such that $u(\mathbf{x})$ admits unit mean. Slip/no-slip phenomena enter Eq. (49) as a boundary condition for u at the solid walls of the channel. For no-slip flows, the boundary condition is of the Dirichlet type,

$$u(\mathbf{x})|_{x\in\partial\Sigma} = 0, \tag{50}$$

while for slip flows is of mixed nature

$$\gamma\frac{\partial u(\mathbf{x})}{\partial n_e} + u(\mathbf{x})|_{\mathbf{x}\in\partial\Sigma} = 0, \tag{51}$$

where γ is the nondimensional slip length. For $\gamma=0$, Eq. (51) reduces to the Dirichlet condition Eq. (50).

Due to the different spectral problem, it can be expected that the density of states $N_{\mathrm{DOS}}(k)$ associated with Eqs. (47)–(51) admit an asymptotic expansion characterized by slightly different properties than that for the Weyl's problem involving the (bare) Laplacian operator Eq. (45).

Figure 10(a) shows $N_{\mathrm{DOS}}(k)$ vs k for the weighted Laplacian [associated with Eqs. (47)–(51)) in a 2D no-slip Poiseuille flow, compared with the leading-order term $N_0(k)=k/\pi$ of the Weyl's problem. The following observations can be derived: (i) $N_{\mathrm{DOS}}(k)\sim k$ even for the weighted Laplacian (as expected, also from the data depicted in Fig. 4); however (ii) the leading-order term $N_0(k)$ of the bare Laplacian operator overestimates $N_{\mathrm{DOS}}(k)$ for the weighted Laplacian. The latter observation is further supported by the data depicted in Fig. 10(b), showing the difference $N_{\mathrm{DOS}}(k)-N_0(k)$ vs k for the 2D Poiseuille flow at different values of γ corresponding to no-slip and slip conditions. It follows from the data depicted in Fig. 10(b) that

$$N_{\mathrm{DOS}}(k) - N_0(k) = -a(\gamma)k, \tag{52}$$

where $a(\gamma)>0$ and depends on the nondimensional slip length γ. Table I reviews the best fit for $a(\gamma)$ in the case of 2D Poiseuille flows. As can be expected $a(\gamma)$ is a decreasing function of γ, since the weight $u(y)$ becomes more uniform as γ increases and tends to 1 for $\gamma\to\infty$. In this case the weighted Laplacian problem reduces to the classical Weyl's problem.

TABLE I. Correction prefactor $a(\gamma)$ to the leading-order term of the density of states for the 2D Poiseuille at different nondimensional slip lengths γ.

γ	$\alpha(\gamma)$
0	1.18×10^{-2}
0.01	9.5×10^{-3}
0.03	6.8×10^{-3}

In order to perform a semianalytical analysis of the problem, it is convenient to consider the family of 2D shear flows,

$$u(y) = \frac{2(\gamma+y)}{2\gamma+1}, \tag{53}$$

possessing unit mean velocity. The parameter γ in Eq. (53) is the nondimensional slip length. For $\gamma=0$, Eq. (53) reduces to the 2D no-slip shear flow possessing unit mean velocity.

For this family of flows the eigenvalues λ_n of the weighted Laplacian operator Eqs. (14) and (15) are given by

$$\lambda_n = \frac{(1+2\gamma)\mu_n^3}{2}, \tag{54}$$

where μ_n are the solutions of the cardinal equation $f(\mu)=0$, where

$$f(\mu) = \mathrm{Ai}'(-\gamma\mu)\mathrm{Bi}'(-(1+\gamma)\mu) - \mathrm{Ai}'(-(1+\gamma)\mu)\mathrm{Bi}'(-\gamma\mu) = 0, \tag{55}$$

expressed in terms of the Airy function $\mathrm{Ai}(\xi)$, $\mathrm{Bi}(\xi)$ of the first and second kind [19], where $\mathrm{Ai}'(\xi)=d\mathrm{Ai}(\xi)/d\xi$, and we used the notation $\mathrm{Ai}'(\xi_1)=d\mathrm{Ai}'(\xi)/d\xi|_{\xi=\xi_1}$, with $\xi_1=-\gamma\mu$ or $-(1+\gamma)\mu$. Similarly for $\mathrm{Bi}(\xi)$.

The corresponding eigenfunctions $\psi_n(y)$ can be expressed as

$$\psi_n(y) = C_n\left[\mathrm{Ai}(-\mu_n(y+\gamma)) - \frac{\mathrm{Ai}'(-\gamma\mu_n)}{\mathrm{Bi}'(-\gamma\mu_n)}\mathrm{Bi}(-\mu_n(y+\gamma))\right], \tag{56}$$

where C_n are normalization factors.

The spectrum can be thus computed accurately even for large n, by enforcing the asymptotic expansions of the Airy functions for negative arguments [19],

$$\mathrm{Ai}(-\xi) \simeq \pi^{-1/2}\xi^{-1/4}\cos\left(\frac{2}{3}\xi^{3/2} - \frac{\pi}{4}\right),$$

$$\mathrm{Bi}(-\xi) \simeq -\pi^{-1/2}\xi^{-1/4}\sin\left(\frac{2}{3}\xi^{3/2} - \frac{\pi}{4}\right). \tag{57}$$

Figure 11(a) depicts the difference $N_0(k)-N_{\mathrm{DOS}}(k)$ for the family of 2D shear flows Eq. (53), up to $k=10^6$. The leading-order term in the expansion of the density of states of the weighted Laplacian, in the presence of a weight $u(y)$ that is solution of a Stokes problem, is different from $N_0(k)=1/\pi$ and is given by

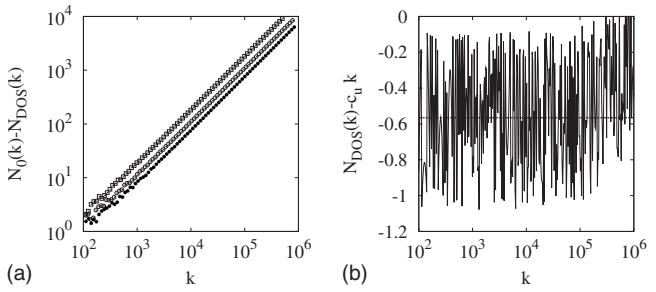

FIG. 11. (a) $N_0(k)-N_{\mathrm{DOS}}(k)$ vs k for the no-slip and slip 2D shear flows. Symbols (□) refer to $\gamma=0$ (no-slip), (○) to $\gamma=0.1$, (●) to $\gamma=0.2$. (b) Next to the leading-order term $N_{\mathrm{DOS}}(k)-c_u k$ vs k for the 2D no-slip shear flow. Dotted line is the mean value equal to −0.565.

$$N_{\mathrm{DOS}}(k) \simeq c_u k, \quad c_u = 1/\pi - a(\gamma), \tag{58}$$

where $a(\gamma)$ is a decreasing function of the nondimensional slip length (as discussed above). The values of $a(\gamma)$ for the family of slip shear flows are reviewed in Table II. Let us analyze the subleading term. The behavior of $N_{\mathrm{DOS}}(k)-c_u k$ is depicted in Fig. 11(b). This difference is approximately constant and negative. This is just the opposite than in the case of the bare Laplacian, where the subleading contribution is positive for the Neumann conditions. This result is however not surprising, just because the presence of an axial weight $u(\mathbf{x})$ makes the eigenvalue problem completely different from the classical Weyl's problem.

V. CONCLUDING REMARKS

The eigenfunctions of the weighted Laplacian embed information on the local structure of the near-wall velocity profile, and a qualitative difference is observed in the scaling of the c spectrum for higher-order eigenfunctions Eqs. (38) and (39). From the analysis developed in this article, it is clear that Eqs. (38) and (39) hold for generic physically realizable channel flow, for which $u(y)>0$ in the open interval (0,1), and such that $u(y)$ behaves linearly as a function of $y-y_{\mathrm{wall}}$, where $y_{\mathrm{wall}}=0,1$.

Quantitative difference between slip and no-slip flows can be detected from the scaling of the density of states of the weighted Laplacian, since the prefactor of the leading-order term depends on the slip length.

Even though the analysis developed in this article does not provide a direct practical criterion for discriminating the possible occurrence of slip (to this purpose, moment analysis of a wide-bore chromatographic experiment is significantly simpler and experimentally feasible), the results obtained provide one more connection between the spectral features of an advection-diffusion operator (which in the present case, expresses the simplest form of interaction between molecular and convective transport) and a physically relevant issue, such as the occurrence of slip velocity. The importance of establishing such connection should not be underestimated, as it allows to interpret a variety of results associated with different experimental conditions on the basis of properties (such as the c spectrum), which depend exclusively on the interaction between advection and diffusion with no reference to the operating conditions, such as, e.g., the form of the injection loading at the channel entrance.

From the structure of the eigenfunctions $\{\psi_h\}$ it is possible to analyze and predict the dispersion properties in the convection-dominated regime, which differ qualitatively from the Taylor-Aris scaling.

Moreover, the analysis of the eigenfunctions of the weighted Laplacian proposed in this article can be extended to approach and interpret a variety of other different transport problems in simple flow systems, such as the effect of mixing of two-fluid stream in pressure-driven microchannels (T junctions) [20], as well as the role of cross-channel geometry on mixing in these systems.

As a final comment, we remark that, depending on the specific transport problem under investigation, different linear operators can be defined for analyzing and predicting the interplay between advection and diffusion in simple flows (compare the present approach with the analysis developed in [4] and in [21]), and the corresponding eigenvalues/eigenfunctions provide complementary information on different phenomenologies associated with mixing, dispersion, homogenization.

TABLE II. Correction prefactor $a(\gamma)$ to the leading-order term of the density of states for the 2D shear flows at different nondimensional slip lengths γ.

γ	$\alpha(\gamma)$
0	1.82×10^{-2}
0.05	1.35×10^{-2}
0.1	1.1×10^{-2}
0.15	9.0×10^{-3}
0.2	7.5×10^{-3}

[1] C.-H. Choi, J. A. Westin, and K. S. Breuer, Phys. Fluids **15**, 2897 (2003); E. Lauga and H. A. Stone, J. Fluid Mech. **489**, 55 (2003).

[2] D. C. Tretheway and C. Meinhart, Phys. Fluids **14**, L9 (2002); P. Huang, J. S. Guasto, and K. Breuer, J. Fluid Mech. **566**, 447 (2006).

[3] C. Neto, D. R. Evans, E. Bonaccurso, H.-J. Butt, and V. S. J. Craig, Rep. Prog. Phys. **68**, 2859 (2005).

[4] M. Giona, S. Cerbelli, and F. Creta, J. Fluid Mech. **612**, 387 (2008).

[5] Ch.-H. Fischer and M. Giersig, J. Chromatogr. A **688**, 97 (1994); M. Harada, T. Kino, T. Masudo, and T. Okada, Anal. Sci. **21**, 491 (2005); T. Okada, M. Harada, and T. Kido, Anal. Chem. **77**, 6041 (2005).

[6] A. Adrover, S. Cerbelli, F. Garofalo, and M. Giona, Anal. Chem. **81**, 8009 (2009). This article analyzes of the shape of outlet chromatograms for high Péclet numbers, and provides a justification of the scaling of the outlet variance. Moreover, it addresses quantitatively the use of wide-bore chromatography as an analytical tool for indirect velocimetric analysis in microchannels.

[7] N. Dyson, *Chromatographic Integration Methods*, 2nd ed. (RCS, Cambridge, 1998).

[8] D. Edwards and H. Brenner, *Macrotransport Processes* (Butterworth-Heinemann, Stoneham, MA, 1993).

[9] H. P. Baltes and E. R. Hilf, *Spectra of Finite Systems* (Bibliographisches Institut, Zürich, 1976).

[10] M. Kac, Am. Math. Monthly **73**, 1 (1966).

[11] B. Sapoval, Th. Gobron, and A. Margolina, Phys. Rev. Lett. **67**, 2974 (1991); J. Kigami and M. L. Lapidus, Commun. Math. Phys. **158**, 93 (1993); M. L. Lapidus and C. Pomerance, Proc. London Math. Soc. **s3-66**, 41 (1993); C. Even, S. Russ, V. Repain, P. Pieranski, and B. Sapoval, Phys. Rev. Lett. **83**, 726 (1999).

[12] G. I. Taylor, Proc. R. Soc. London, Ser. A **219**, 186 (1953); R. Aris, *ibid.* **235**, 67 (1956).

[13] R. B. Bird, W. E. Stewart, and E. N. Lightfoot, *Transport Phenomena*, 2nd ed. (Wiley, New York, 2002).

[14] This result stems from a detailed numerical analysis of the advection-diffusion problem for channel possessing aspect ratio $\alpha \geq 5$, by solving the complete advection-diffusion equation Eq. (2), enforcing both the infinite-column approximation and the Danckwerts condition. For fixed $\mathrm{Pe}_{\mathrm{eff}}$, the accuracy of the approximation in which axial diffusion is neglected improves as the aspect ratio α increases.

[15] The integrals Eq. (8) converge for any finite value of $\mathrm{Pe}_{\mathrm{eff}}$. For 2D straight channels, and 3D circular channels in the presence of no-slip boundary conditions (Poiseuille flow), it can be proved that, for $n \geq 2$, $m_{\mathrm{out}}^{(n)} \sim \mathrm{Pe}_{\mathrm{eff}}^{(n-1)/3}$, while $m_{\mathrm{out}}^{(1)} \sim \log \mathrm{Pe}_{\mathrm{eff}}$, as discussed in Sec. III. In the presence of slip boundaries, the nth moment for any $n \geq 1$ converges for $\mathrm{Pe}_{\mathrm{eff}} \to \infty$ towards a constant value corresponding to the nth moment of the purely kinematic residence-time distribution.

[16] The eigenvalues/eigenfunctions have been obtained numerically by expanding $\psi(y)$ in cosines, $\psi(y) = \Sigma_{k=0}^{N} x_k \cos(k\pi y)$, and by solving the generalized eigenvalue problem $-\lambda \mathbf{Bx} = \mathbf{Ax}$, where $\mathbf{x} = (x_0, x_1, \ldots, x_N)$, $\mathbf{A} = (A_{h,k} = -(\pi h)^2 s_h \delta_{h,k})$, $s_0 = 1$, $s_h = 1/2$, $h \geq 1$, $\mathbf{B} = (B_{h,k} = \int_0^1 u(y) \cos(h\pi y) \cos(k\pi y) dy)$.

[17] The fact that $\lim_{\varepsilon \to 0}(\varepsilon) = r_0$ approaches a constant value derives from the most critical situation for the c spectrum expressed by Eq. (38). The observation $r_0 \sim \mathcal{O}(10^{-1})$ for no-slip Poiseuille flow is numerical.

[18] R. Balian and C. Bloch, Ann. Phys. **60**, 401 (1970).

[19] N. N. Lebedev, *Special Functions & Their Applications* (Dover, New York, 1972).

[20] R. F. Ismagilov, A. D. Stroock, P. J. A. Kenis, G. Whitesides, and H. A. Stone, Appl. Phys. Lett. **76**, 2376 (2000); J.-B. Salmon and A. Ajdari, J. Appl. Phys. **101**, 074902 (2007).

[21] M. Giona and S. Cerbelli, Phys. Rev. E **78**, 046303 (2008); M. Giona, S. Cerbelli, and F. Garofalo, EPL **83**, 34001 (2008).